Journal of Materials Chemistry C

PAPER

View Article Online
View Journal | View Issue

Cite this: J. Mater. Chem. C, 2015, 3, 4345

γ radiation induced self-assembly of fluorescent molecules into nanofibers: a stimuli-responsive sensing†

Ji-Min Han,[a] Na Wu,[a] Brian Wang,[b] Chen Wang,[a] Miao Xu,[a] Xiaomei Yang,[a] Haori Yang[c] and Ling Zang*[a]

Received 3rd March 2015,
Accepted 23rd March 2015

DOI: 10.1039/c5tc00594a

www.rsc.org/MaterialsC

Low dose detection of γ radiation remains critical for radiology therapy and nuclear security. We report herein on a novel dual-band fluorescence sensor system based on a molecule, 4-(1*H*-phenanthro[9,10-*d*]-imidazol-2-yl)-*N*,*N*-diphenylaniline (PI-DPA), which can be dissolved into halogenated solvents to enable expedient detection of γ radiation. The limit of detection was projected down to 0.006 Gy. Exposure to γ radiation decomposes $CHCl_3$ into small radicals, which then combine to produce HCl. Strong interaction of HCl with the imidazole group of PI-DPA converts it into a PI-DPA–HCl adduct, which self-assembles into nanofibers, quenching the fluorescence of the pristine PI-DPA molecule, while producing new fluorescent emission at longer wavelength. Such dual-band emission response provides improved sensing reliability compared to single band response. Systematic investigations based on acid titration, ^{1}H NMR spectral measurements and time-course SEM imaging suggest that the observed new fluorescence band is due to π–π stacking of the PI-DPA–HCl adduct, which is facilitated by the formation of hydrogen bonded cluster units. The nanofibers exhibited high and reversible photoconductivity. Combining with the sensitive fluorescence response, the photoconductive nanofibers will enable development of a multimode stimuli-responsive sensor system that is suited for small, low cost dosimetry of γ radiation with improved sensitivity and detection reliability.

Introduction

Low dose detection and dosimetry of γ radiation is crucial for radiology therapy, nuclear security and space mission.[1] Current detection technologies are vulnerable to low sensitivity (ion chambers),[2] energy and angular dependence (semiconductor detectors),[3] expensive and/or complicated manufacturing (scintillation detectors),[4] and time-consuming for read out (film-based detectors).[1a] Aiming to overcome these problems, various chemical sensors have been developed to detect γ radiation. Of the chemical sensors developed thus far, fluorescent sensing represents a simple, rapid, and highly sensitive approach.[5] Among these studies, most of the efforts were focused on the fluorescence "turn-off" (quenching) mechanism. Recently, we have reported an imidazole-based sensor molecule, which can be dissolved into halogenated solvents (*e.g.*, $CHCl_3$) to enable instant detection of γ radiation.[5h] The sensing mechanism was based on fluorescence quenching caused by the chemical interaction between the sensor molecule and HCl molecule produced from γ-radiation decomposition of $CHCl_3$. However, such single emission band monitoring faces potential challenge regarding detection reliability. For example, some environmental interferences or even excitation light fluctuation may cause the emission intensity decrease, resulting in false positives of radiation detection. To this regard, fluorescence turn-on sensors would be more ideal compared to the quenching based ones, though few of such turn-on sensors have been reported. Difficulty in development of fluorescence turn-on sensors for radiation detection mostly lies in the molecular design, for which the sensor molecule must be sufficiently reactive to the signature species formed under γ radiation, whereas the reaction product thus formed must be highly fluorescent and more importantly robust enough against any fluorescence quenching reaction with γ radiation or the reactive radicals produced.

We report herein on a new fluorescence turn-on sensor system based on molecular self-assembly as shown in Scheme 1, where

[a] Nano Institute of Utah, Department of Materials Science and Engineering, University of Utah, 36 South Wasatch Dr., Salt Lake City, Utah 84112, USA. E-mail: lzang@eng.utah.edu
[b] Department of Radiation Oncology, University of Louisville, 529 South Jackson Street, Louisville, Kentucky 40202, USA
[c] Department of Nuclear Engineering & Radiation Health Physics, Oregon State University, 3451 SW Jefferson Way, Radiation Center E108, Corvallis, Oregon 97331, USA

† Electronic supplementary information (ESI) available: Materials, general instrumentation, and control experiments. See DOI: 10.1039/c5tc00594a

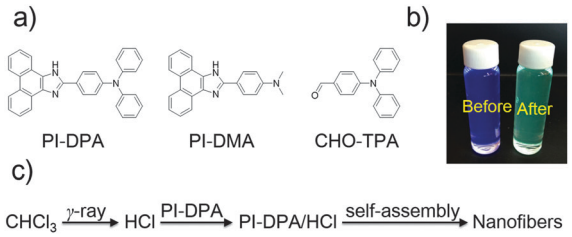

Scheme 1 (a) Molecular structures of the sensor molecule, PI-DPA, and its two analogues. (b) Fluorescence photographs of a $CHCl_3$ solution of PI-DPA (1×10^{-5} mol L^{-1}) before and after 5 Gy of γ radiation. (c) The dual-band fluorescence sensing mechanism of PI-DPA, which can be combined with the photoconductive (resistive) sensing of nanofibers.

the sensor molecule is 4-(1*H*-phenanthro[9,10-*d*]imidazol-2-yl)-*N*,*N*-diphenylaniline (PI-DPA), which can be dissolved in a halogen solvent like $CHCl_3$. Upon exposure to γ radiation $CHCl_3$ decomposes into radicals, which then combine to produce HCl. Strong interaction of HCl with the imidazole group of PI-DPA converts the molecule to the PI-DPA–HCl adduct, which tends to self-assemble to form a well-defined nanofiber structure. To the best of our knowledge, this is the first report on the nanofibril self-assembly induced by γ radiation. Formation of the nanofibril structure quenches the fluorescence of the pristine PI-DPA molecule, and generates a new fluorescence band at longer wavelength intrinsic to the aggregation state, providing a dual-band fluorescence sensing. By monitoring both the emission quenching and turn-on, the detection specificity or reliability of γ radiation is much enhanced (compared to the single band fluorescence quenching). Furthermore, by measuring the intensity increase of the new emission band, the detection sensitivity can potentially be improved by taking advantage of the low emission intensity (background) at that wavelength of the pristine sensor molecule.[6] Moreover, the aggregation state helps prevent further molecular reaction with γ radiation or the reactive radicals produced. Remarkably, the long nanofibers exhibited high and reversible photoconductivity, providing another signal output to monitor γ radiation. A conductivity based gamma radiation sensor was previously reported using polymer–carbon nanotube composites,[7] though the detection sensitivity was not competitive, in the range of 10 Gy (or 10^3 rad).

Results and discussion

The sensor response of PI-DPA was first investigated by UV-vis and fluorescence spectral measurements. As shown in Fig. 1a, the main absorption peak of PI-DPA centered at 370 nm gradually red shifted to 393 nm with increasing dose of γ radiation. Consistent with the absorption change, a dramatic fluorescence spectral change was also observed concurrently (Fig. 1b). Before exposure to γ radiation the $CHCl_3$ solution of PI-DPA demonstrated a strong blue fluorescence at 420 nm, whereas such emission was gradually quenched with increasing dose of γ radiation. Meanwhile, a new fluorescence band emerged at a longer wavelength, centered at 494 nm. Remarkably, both the

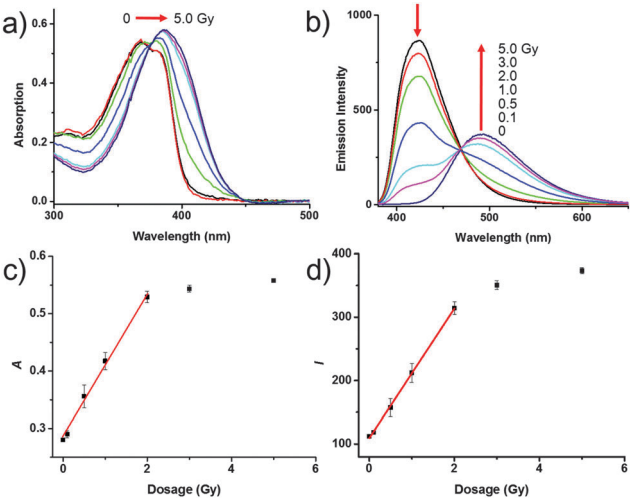

Fig. 1 (a) The absorption and (b) fluorescence spectra of PI-DPA in a $CHCl_3$ solution (1×10^{-5} mol L^{-1}) before and after exposure to varying doses of γ radiation (0–5.0 Gy). The excitation wavelength is 370 nm. (c) Absorption change of PI-DPA recorded at 393 nm and (d) fluorescence intensity change recorded at 494 nm, both as a function of the dose of γ radiation.

absorption and fluorescence of PI-DPA showed a significant change after only 0.1 Gy of radiation, implying the high sensitivity of sensor response. All the spectral changes were observed instantly (in seconds) after the irradiation, indicating fast sensor response. Interestingly, both the absorption and emission intensity (at 494 nm) showed a linear relationship with the radiation dose in the low range (0–2.0 Gy) as shown in Fig. 1c and d, which allows for quantitative data analysis to determine the detection limit. By defining an intensity (or absorbance) change three times higher than the standard deviation (σ) as the detectable signal, the detection limit (based on 3σ/slope) for the sensor solution shown in Fig. 1 can already reach 0.006 Gy through the emission intensity measurement, or 0.008 Gy through the absorption measurement (see detailed data processing in ESI†).[5h,8]

Both the red shifted absorption and new fluorescence band shown in Fig. 1 imply molecular aggregation of PI-DPA as indeed observed by dynamic light scattering (DLS) measurement of the solution after 5 Gy γ irradiation (Fig. S2, ESI†). To explore the microscopic morphology of the molecular aggregation, the precipitation of PI-DPA molecules was transferred onto a glass substrate by drop-casting. Long, well-defined nanofibers were observed using an optical microscope as shown in Fig. 2. The bright field image (Fig. 2a) demonstrates clearly the individual PI-DPA nanofibers, as well as the bundles of several nanofibers. One possible mechanism causing such fibril aggregation is through the formation of a triarylamine radical, which was proven to be effective for initiating the molecular assembly of neutral triarylamine molecules through synergistic π–π stacking and charge transfer interactions.[9] Considering that PI-DPA contains a triarylamine moiety, triarylamine radicals may also be formed in our case either by direct interaction with γ radiation or by reacting with the radicals decomposed from $CHCl_3$. However, the strong green

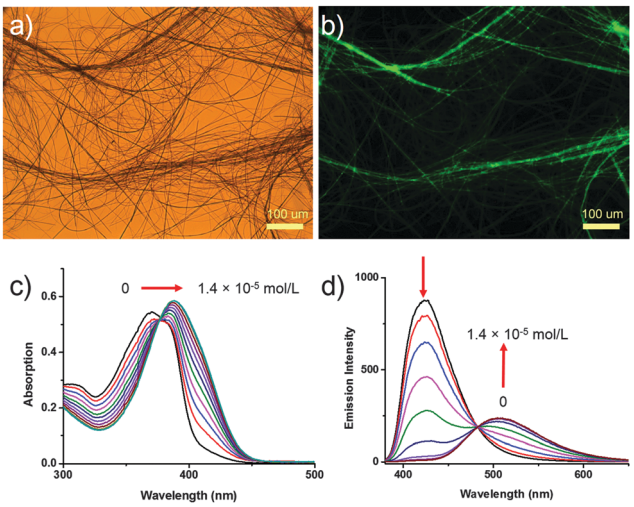

Fig. 2 (a) Bright-field and (b) fluorescence optical microscopy images of the nanofibers assembled from PI-DPA (1×10^{-5} mol L^{-1} in $CHCl_3$) after 5 Gy of γ radiation, deposited on a glass slide; (c) absorption and (d) fluorescence spectra of PI-DPA in $CHCl_3$ solution (1×10^{-5} mol L^{-1}) upon titration with a series of concentration of HCl (0, 0.2, 0.4, 0.6, 0.8, 1.0, 1.2 and 1.4 $\times$ 10^{-5} mol L^{-1}). The excitation wavelength is 370 nm.

fluorescence of the PI-DPA nanofibers thus formed (Fig. 2b) excludes the presence of triarylamine radicals, as the cationic radicals (if present) would function as strong fluorescence quenchers. To further exclude the radical mediating pathway, we performed the same experiments as that shown in Fig. 1 with a reference compound, CHO-TPA (Scheme 1), which contains the same trarylamine group as PI-DPA, but lacks the imidazole group. In comparison, there was no significant fluorescence change observed even after 5 Gy of γ radiation (Fig. S3, ESI†), indicating that no aggregation or structural change occurred in the molecule, thus excluding the possibility of triarylamine radical mediated aggregation. These experimental results clearly suggest that the observed molecular aggregation of PI-DPA under γ radiation is unlikely due to the formation of triarylamine radicals; rather the imidazole group seems to play a crucial role in the molecular assembly.

An alternative mechanism for the observed molecular aggregation of PI-DPA is through the interaction between the imidazole group and HCl produced from the γ irradiated $CHCl_3$.[5h,10] To confirm the HCl mediated molecular aggregation, we carried out a series of HCl titration experiments with the same $CHCl_3$ solution of PI-DPA as used in the γ radiation experiment. As expected, upon addition of HCl both the absorption and fluorescence spectra of PI-DPA (Fig. 2c and d) underwent almost identical spectral changes as observed under γ radiation (Fig. 1a and b). Both the absorption and fluorescence spectral changes were observed instantly upon addition of HCl, indicating the fast acid–base binding interaction between HCl and the imidazole moiety. This fast bimolecular reaction ensures the quick sensor response. Moreover, the formation of the PI-DPA–HCl adduct is a reversible reaction, which can be dissociated back to the pristine PI-DPA molecule simply by adding a strong base. As shown in Fig. S4 (ESI†), the fluorescence spectra of the γ irradiated PI-DPA suspension was nearly fully recovered by adding Et_3N. This further indicates that the observed spectral change of PI-DPA was solely due to the binding with HCl. The PI-DPA solution in $CHCl_3$ with excess of HCl was also cast onto a quartz slide to measure the solid state (thin film) fluorescence spectra. As shown in Fig. S5 (ESI†), the fluorescence spectrum obtained matches very well the spectra measured over the PI-DPA solution after 5 Gy of γ radiation (Fig. 1b) and the same solution after addition of HCl (Fig. 2d). On the other hand, if the same titration experiment was performed in a good solvent like DMSO, where the protonated PI-DPA is soluble (no aggregation formed), only a slight decrease in fluorescence intensity was observed and no new band emerged at longer wavelength (Fig. S6, ESI†). These comparative measurements again indicate that the observed fluorescence spectral shift is mainly due to the HCl binding induced molecular aggregation.

The HCl titration curves shown in Fig. 2 can be used to estimate the concentration of HCl formed at different doses of γ radiation by comparing the absorption or fluorescence intensity change. For instance, the fluorescence intensity increase measured at 494 nm after 1 Gy of γ radiation (Fig. 1b) corresponds approximately to the fluorescence intensity upon addition of 6×10^{-6} mol L^{-1} of HCl (Fig. 2d), implying that the concentration of HCl produced at 1 Gy of γ radiation was about 6×10^{-6} mol L^{-1}. This value is in good agreement with the theoretically projected concentration of HCl (8×10^{-6} mol L^{-1}) produced under the same conditions.[10b]

As a control, we also synthesized an analogue of PI-DPA, by replacing the two phenyl groups with two methyl groups. The analogue (namely PI-DMA, Scheme 1) was also examined for the same γ radiation and HCl titration experiments as performed for PI-DPA. However, no fibers or any aggregates were formed from the PI-DMA solution. Under continuous γ radiation, the fluorescence of PI-DMA in $CHCl_3$ was increased in intensity (in contrast to the decrease observed for PI-DPA), and no new fluorescence band emerged at longer wavelength (Fig. S7, ESI†). The observed fluorescence intensity increase is due to the acidification of PI-DMA.[11] These control experiments further confirm that the significant fluorescence spectral shift observed for PI-DPA is mostly caused by the molecular aggregation, for which the two phenyl rings in PI-DPA likely play a critical role in the π–π stacking intermolecular arrangement, which in turn enables formation of a nanofiber structure (*vide infra*).

In addition to the high sensitivity, the PI-DPA sensor system also exhibited excellent selectivity to γ radiation compared to the common UV radiation or sunlight, which often cause fluorescence quenching of molecular sensors through photo-oxidation (Fig. S8, ESI†). Upon exposure to UV radiation or sunlight both the absorption and fluorescence of PI-DPA decrease in intensity, while in both cases the spectral shape remains unchanged, indicating that some portion of the PI-DPA molecules were converted to the non-fluorescent state (structure) *via* photo-oxidation. Moreover, such photoinduced conversion was not reversible, *i.e.*, the decreased absorption or fluorescence could not be recovered by addition of base.

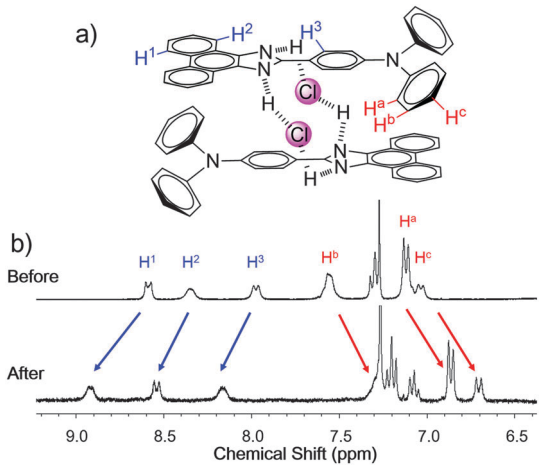

Fig. 3 (a) The proposed HCl assisted π–π stacking aggregation of PI-DPA molecules; (b) partial ^{1}H NMR spectra ($CDCl_3$) of PI-DPA (2 mmol) before and after the addition of HCl (20 mmol).

The characteristic dual-band fluorescence response to γ radiation makes PI-DPA a unique sensor molecule for selective detection of γ radiation against the interference from UV or sunlight irradiation. This is superior to the common fluorescence sensors based on single band quenching mode, which may produce false positive for γ radiation when exposed to UV or sunlight.

Using X-ray crystallography, Yoshida *et al.* revealed that the PI-DPA molecules can exhibit enhanced π–π stacking ability in acetic acid (HAc), through a hydrogen bonded cluster unit composed of two PI-DPA (as hosts) and two HAc (as guests).[12] Considering the fact that hydrogen bonding interaction can help control the organization of aromatic rings in face-to-face π–π stacking,[13] we assume that the PI-DPA–HCl adduct can form a similar π–π stacking assembly to PI-DPA–HAc (Fig. 3a and Fig. S9a, ESI†). To verify this hypothesis, we first characterized the self-assembly of the PI-DPA–HAc adduct by the ^{1}H NMR spectra (Fig. S9b, ESI†). Upon addition of HAc, the three signals assigned to the protons on one of the phenyl groups connected to the amine, H^a (7.10 ppm), H^b (7.59 ppm) and H^c (7.01 ppm), experienced upfield shifting. These NMR spectral shifts are due to the shielding from the aromatic ring current of the neighboring phenanthryl group within the assembly, which is characteristic of the π–π stacking interaction.[14] The signals at 8.61 ppm (H^1), 8.37 ppm (H^2) (assigned to the two protons on the phenanthryl ring), and 7.98 ppm (H^3) (assigned to the proton on the central phenyl ring connected to imidazole) experienced slight shifting, resulting from the competition between π–π stacking and aromatic C–H···Ac^- interaction.[15] The NMR spectral changes in Fig. S9b (ESI†) are highly consistent with the hydrogen bonding assisted π–π stacking cluster structure reported for the assembly of the PI-DPA–HAc adduct. In comparison, we examined the NMR spectral change of the PI-DPA–HCl adduct under the same conditions (Fig. 3b). Upon addition of HCl the signals of H^a, H^b, and H^c showed significant upfield shifting (the same as in the case of PI-DPA–HAc), indicating the strong π–π stacking interaction. However, the signals of H^1, H^2, and H^3 were shifted downfield, to 8.92 ppm, 8.52 ppm and 8.18 ppm, respectively, likely due to the stronger aromatic C–H···Cl^- hydrogen bonds compared to the weak aromatic C–H···Ac^- interactions.[16] The consistent ^{1}H NMR spectral shift between PI-DPA–HCl and PI-DPA–HAc adducts (particularly the upfield shifting due to π–π stacking) suggests that the molecular assembly of PI-DPA–HCl adopts a similar intermolecular arrangement configuration to that revealed by the crystalline structure of PI-DPA–HAc. Such HCl assisted assembly is shown in Fig. 3a, wherein the π–π stacking self-assembly is enhanced by the hydrogen bonded cluster unit of two PI-DPA and two HCl. The flexible angle of H···Cl···H bonding[16d] facilitates the formation of a HCl bridging structure.

To monitor the molecular aggregation process, time-course scanning electron microscopy (SEM) imaging was performed over the samples drop cast from the PI-DPA solution at different time intervals after addition of HCl. As shown in Fig. 4, small particles were quickly formed within 2 minutes after addition of HCl, indicating the fast molecular aggregation (nucleation) process facilitated by HCl binding. These small particles then grow into a larger phase, here a nanofiber structure, mainly driven by the one-dimensional π–π stacking arrangement.[17d,18] Upon further aging, elongated nanofibers can be formed with

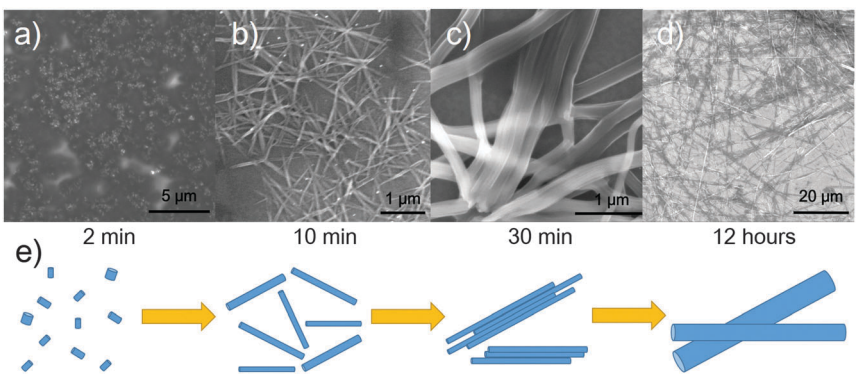

Fig. 4 SEM images of samples drop cast on a silicon wafer from a PI-DPA solution (1×10^{-5} mol L^{-1} in CH_2Cl_2) at varying time intervals after addition of 20 fold excess of HCl: (a) 2 min, (b) 10 min, (c) 30 min, and (d) 12 hours. The CH_2Cl_2 solvent was used instead mainly because of its higher volatility; the faster vaporization helps minimize the additional aggregation formed during the drying process on the surface. (e) Schematic drawing of the nanofibers growth process.

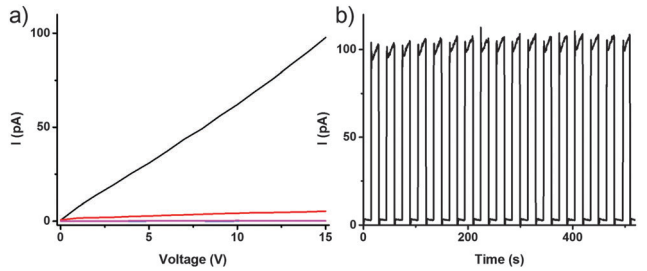

Fig. 5 (a) *I–V* curves measured over the PI-DPA nanofibers in the dark (red) and under white light irradiation with a power density of 0.25 mW mm^{-2} (black). In comparison, the films of neutral PI-DPA (pink) and PI-DPA–HCl nanoparticles (blue) showed almost no photocurrent under the same light conditions (two curves are overlapped at the bottom of the plot); (b) photocurrent of PI-DPA nanofibers measured at 15 V bias in response to turning on and off the white light irradiation, showing a fast, reversible photo-response.

length growing up to the millimetre range. In contrast, the neutral PI-DPA solution (without addition of HCl) forms only a film structure when cast on the same substrate (Fig. S9, ESI†), whereas no discrete aggregates were found. These results clearly demonstrate that the HCl binding facilitates the molecular aggregation, and the HCl bridged π–π stacking arrangement drives the one-dimensional phase growth into a well-defined fibril structure.

Nanofibers self-assembled from molecules through π–π stacking usually demonstrate unique electrical properties compared to the amorphous bulk (or film) materials.[17,18] For example, the one-dimensional molecular arrangement can facilitate the charge transport along the long axis of the nanofiber, mainly through π-electron delocalization mediated by the intermolecular π–π stacking as previously evidenced by both theoretical and experimental observations.[19] With the efficient charge transport pathway along the nanofiber, we attempted to explore the photoconductivity of PI-DPA nanofibers. As shown in Fig. 5a, the nanofibers generated from the γ irradiation exhibited low current in the dark, in the range of pA. Such low conductivity is usually observed for pure organic materials self-assembled from molecules, considering the minimal doping.[20] Remarkably, under white light irradiation at a power density of 0.25 mW mm^{-2} the photocurrent increased by over one order of magnitude, reaching the range of hundred pA. The increased conductivity observed under light is likely due to the photo-induced charge separation between the nanofiber and surface adsorbed oxygen, in conjunction with the efficient charge transport along the nanofiber. Oxygen is often employed for increasing the concentration of holes in p-type organic materials.[20a,21] The LUMO levels of both PI-DPA (−1.4 eV *vs.* vacuum, calculated, see ESI†) and the PI-DPA–HCl adduct (−2.1 eV, calculated) are energetically sufficient to drive electron transfer to oxygen upon photo-excitation.

To further verify that the observed photocurrent enhancement for PI-DPA nanofibers is enabled by the π–π stacking mediated charge delocalization, we performed the same photocurrent experiments with the films of neutral PI-DPA and the PI-DPA–HCl nanoparticles (the early stage aggregates shown in Fig. 4a). As expected, the two samples showed almost no photocurrent response under the same light irradiation (Fig. 5a). These results clearly indicate that the nanofiber morphology is pivotal for the high photocurrent response by providing an efficient charge transport pathway. In addition to the high magnitude, the photocurrent response was also found to be fast (in seconds) and reversible (Fig. 5b). Combining such efficient photocurrent measurement with the dual-band fluorescence monitoring as described above will enable development of a multimode stimuli-responsive sensor system based on the γ radiation induced self-assembly of PI-DPA. For example, a small volume of the chloroform solution of the sensor can be sealed in a microfluidic like device (solvent resistive), wherein the nanofibers formed can be aligned *in situ* into a circuit for photocurrent measurement (monitoring). The multimode sensor system thus fabricated is expected to provide not only improved sensitivity, but also better detection reliability.

Conclusions

In summary, we report herein on a new fluorescence sensor system based on γ radiation stimulated self-assembly of a fluorescence molecule, PI-DPA, dispersed in $CHCl_3$. When exposed to γ radiation, HCl is formed by the decomposition of $CHCl_3$; the strong binding interaction between HCl and PI-DPA converts the molecule to the PI-DPA–HCl adduct, which self-assembles into a well-defined nanofiber structure, mainly driven by the hydrogen bonding assisted π–π stacking. As a result, the blue fluorescence emission (420 nm) of the pristine PI-DPA is quenched, while a new emission band of the nanofibers emerged at a longer wavelength (494 nm). This dual-band emission monitoring can help enhance the detection reliability of γ radiation. By fitting linearly the emission intensity increase at 494 nm as a function of radiation dose, we can project the detection limit down to 0.006 Gy, which represents, to the best of our knowledge, the best sensitivity among the chemical sensors reported thus far. The nanofibers of PI-DPA formed under γ radiation demonstrate high photoconductivity, which provides an additional sensor mode to detect γ radiation. Combining with the dual-band fluorescence sensing, the photoconductive nanofibers can be developed into a multimode stimuli-responsive sensor system incorporating both optical and electrical signal modulation. Such a responsive self-assembly sensor may find broad applications in low dose detection of γ radiation, taking advantage of the high sensitivity, fast response, small size and low cost.

Experimental section

Synthesis

PI-DPA: phenanthrene-9,10-quinone (208 mg, 1.0 mmol), ammonium bicarbonate (1.0 g, 13 mmol, excess) and 4-(diphenylamino)benzaldehyde (273 mg, 1.0 mmol) were added into 50 mL of EtOH in a 100 mL round flask; the suspension thus obtained was refluxed for 6 hours. After cooling to room temperature, the

solvent was removed using a rotatory evaporator, and the residue was further purified by column chromatography (silica gel) to obtain PI-DPA as a white solid (337 mg, 73% yield). ^{1}H NMR (DMSO-d_6, 300 MHz, ppm): δ = 13.66 (2 H, bs), 8.90 (4 H, d, J = 8 Hz), 8.65 (4 H, d, J = 8 Hz), 8.5 (4 H, d, J = 8 Hz), 8.11 (4 H, d, J = 8 Hz), 8.79 (4 H, t, J = 8 Hz), 8.68 (4 H, t, J = 8 Hz); ^{13}C NMR (DMSO-d_6, 75 MHz, ppm): δ = 149.6, 140.6, 130.5, 128.5, 128.0, 127.9, 127.6, 126.2, 124.8, 122.9. LRMS (ESI): m/z calcd: 461.2; found: 462.3 $[M + H]^+$.

γ radiation experiments

Following the method we developed in the previous study,[5h] the γ radiation experiments were performed at room temperature using a 6 MV photon beam on a Novalis Classic Linear Accelerator (LINAC) (BrainLAB AG, Feldkirchen, Germany). The radiation output was calibrated using an ionization chamber to generate 0.01 Gy per MU (Monitor Unit) at a maximum dose depth of 1.4 cm in water with a Source to Surface Distance (SSD) of 100 cm. The ionization chamber used has a calibration that is traceable to an Accredited Dosimetry Calibration Laboratory. The radiation beam from the LINAC machine head was angled to the downward direction, wherein the sensor samples were placed underneath at a height that was calculated for a certain dose of radiation. Slabs of solid water were placed atop the samples to provide dose build up. We performed the experiments with varying volumes and heights of solution samples (*i.e.*, using vials of 1–10 mL in volume and 1–6 cm in height), and found that the detection efficiency (in terms of fluorescence quenching percentage under a certain dose of radiation) was almost the same.

Acknowledgements

This work was supported by the Department of Homeland Security, Science and Technology Directorate under grant number (2009-ST-108-LR0005), NSF (CHE 0931466), the SEED grant of the VP office of University of Utah (award # 10029849), and USTAR program.

Notes and references

1 (*a*) G. F. Knoll, *Radiation detection and measurement*, Wiley, 2010; (*b*) R. H. Herz, *The photographic action of ionizing radiations in dosimetry and medical, industrial, neutron, auto- and microradiography*, Wiley-Interscience, New York, 1969.

2 S. C. Graham, R. H. Friend, S. Fung and S. C. Moratti, *Synth. Met.*, 1997, **84**, 903–904.

3 J. G. Webster, *The Measurement, Instrumentation, and Sensors: Handbook*, CRC Press, 1999.

4 L. Storm and H. I. Israel, *At. Data Nucl. Data Tables*, 1970, **7**, 565–681.

5 (*a*) E. A. B. Silva, J. F. Borin, P. Nicolucci, C. F. O. Graeff, T. G. Netto and R. F. Bianchi, *Appl. Phys. Lett.*, 2005, **86**, 131902; (*b*) A. Singh, K. Chen, S. J. Adelstein and A. I. Kassis, *Radiat. Res.*, 2007, **168**, 233–242; (*c*) H. Zhong, Y. Zhao, Y. Li and Q. Pei, *Nanotechnology*, 2008, **19**, 505503; (*d*) Y. S. Zhao, H. Zhong and Q. Pei, *Phys. Chem. Chem. Phys.*, 2008, **10**, 1848–1851; (*e*) Z. Li, S. Wu, J. Han and S. Han, *Analyst*, 2011, **136**, 3698–3706; (*f*) E. S. Bronze-Uhle, A. Batagin-Neto, F. C. Lavarda and C. F. O. Graeff, *J. Appl. Phys.*, 2011, **110**, 073510; (*g*) E. S. Bronze-Uhle, A. Batagin-Neto, D. M. Fernandes, I. Fratoddi, M. V. Russo and C. F. O. Graeff, *Appl. Phys. Lett.*, 2013, **102**, 241917; (*h*) J. M. Han, M. Xu, B. Wang, N. Wu, X. Yang, H. Yang, B. J. Salter and L. Zang, *J. Am. Chem. Soc.*, 2014, **136**, 5090–5096; (*i*) X. Dong, F. Hu, Z. Liu, G. Zhang and D. Zhang, *Chem. Commun.*, 2015, **51**, 3892–3895.

6 L. Basabe-Desmonts, D. N. Reinhoudt and M. Crego-Calama, *Chem. Soc. Rev.*, 2007, **36**, 993–1017.

7 J. M. Lobez and T. M. Swager, *Angew. Chem., Int. Ed.*, 2010, **49**, 95–98.

8 B. M. Tissue, *Basics of Analytical Chemistry and Chemical Equilibria*, John Wiley & Sons, 2013.

9 (*a*) E. Moulin, F. Niess, M. Maaloum, E. Buhler, I. Nyrkova and N. Giuseppone, *Angew. Chem., Int. Ed.*, 2010, **49**, 6974–6978; (*b*) V. Faramarzi, F. Niess, E. Moulin, M. Maaloum, J. F. Dayen, J. B. Beaufrand, S. Zanettini, B. Doudin and N. Giuseppone, *Nat. Chem.*, 2012, **4**, 485–490.

10 (*a*) M. Ottolenghi and G. Stein, *Radiat. Res.*, 1961, **14**, 281; (*b*) H. R. Werner and R. F. Firestone, *J. Phys. Chem.*, 1965, **69**, 840–849.

11 (*a*) J. Dey and S. K. Dogra, *J. Phys. Chem.*, 1994, **98**, 3638–3644; (*b*) H. J. Kim, C. H. Heo and H. M. Kim, *J. Am. Chem. Soc.*, 2013, **135**, 17969–17977.

12 Y. Ooyama, H. Kumaoka, K. Uwada and K. Yoshida, *Tetrahedron*, 2009, **65**, 8336–8343.

13 A. N. Sokolov, T. Friščić and L. R. MacGillivray, *J. Am. Chem. Soc.*, 2006, **128**, 2806–2807.

14 (*a*) A. S. Shetty, J. Zhang and J. S. Moore, *J. Am. Chem. Soc.*, 1996, **118**, 1019–1027; (*b*) Y. Hamuro, S. J. Geib and A. D. Hamilton, *J. Am. Chem. Soc.*, 1997, **119**, 10587–10593; (*c*) J. Y. Wang, J. Yan, Z. Li, J. M. Han, Y. Ma, J. Bian and J. Pei, *Chem. – Eur. J.*, 2008, **14**, 7760.

15 N. H. Evans and P. D. Beer, *Angew. Chem., Int. Ed.*, 2014, **53**, 11716–11754.

16 (*a*) V. S. Bryantsev and B. P. Hay, *J. Am. Chem. Soc.*, 2005, **127**, 8282–8283; (*b*) K. Chellappan, N. J. Singh, I.-C. Hwang, J. W. Lee and K. S. Kim, *Angew. Chem., Int. Ed.*, 2005, **44**, 2899–2903; (*c*) K. J. Winstanley, A. M. Sayer and D. K. Smith, *Org. Biomol. Chem.*, 2006, **4**, 1760–1767; (*d*) A. Kovács and Z. Varga, *Coord. Chem. Rev.*, 2006, **250**, 710–727; (*e*) Y. Li and A. H. Flood, *Angew. Chem., Int. Ed.*, 2008, **47**, 2649–2652; (*f*) V. Havel, J. Svec, M. Wimmerova, M. Dusek, M. Pojarova and V. Sindelar, *Org. Lett.*, 2011, **13**, 4000–4003.

17 (*a*) K. Balakrishnan, A. Datar, R. Oitker, H. Chen, J. Zuo and L. Zang, *J. Am. Chem. Soc.*, 2005, **127**, 10496–10497; (*b*) K. Balakrishnan, A. Datar, T. Naddo, J. Huang, R. Oitker, M. Yen, J. Zhao and L. Zang, *J. Am. Chem. Soc.*, 2006, **128**, 7390–7398; (*c*) Y. Che, A. Datar, K. Balakrishnan and L. Zang, *J. Am. Chem. Soc.*, 2007, **129**, 7234–7235;

(*d*) L. Zang, Y. Che and J. S. Moore, *Acc. Chem. Res.*, 2008, **41**, 1596–1608.

18 (*a*) A. C. Grimsdale and K. Mullen, *Angew. Chem., Int. Ed.*, 2005, **44**, 5592–5629; (*b*) Y. S. Zhao, H. Fu, A. Peng, Y. Ma, Q. Liao and J. Yao, *Acc. Chem. Res.*, 2010, **43**, 409–418; (*c*) F. Wurthner, *Chem. Commun.*, 2004, 1564–1579; (*d*) C. Park, J. E. Park and H. C. Choi, *Acc. Chem. Res.*, 2014, **47**, 2353–2364.

19 (*a*) Y. Che, A. Datar, X. Yang, T. Naddo, J. Zhao and L. Zang, *J. Am. Chem. Soc.*, 2007, **129**, 6354–6355; (*b*) Y. Che, X. Yang, G. Liu, C. Yu, H. Ji, J. Zuo, J. Zhao and L. Zang, *J. Am. Chem. Soc.*, 2010, **132**, 5743–5750; (*c*) Y. Che, H. Huang, M. Xu, C. Zhang, B. R. Bunes, X. Yang and L. Zang, *J. Am. Chem. Soc.*, 2011, **133**, 1087–1091; (*d*) V. Coropceanu, J. Cornil, D. A. da Silva Filho, Y. Olivier, R. Silbey and J. L. Bredas, *Chem. Rev.*, 2007, **107**, 926–952; (*e*) F. S. Kim, G. Ren and S. A. Jenekhe, *Chem. Mater.*, 2011, **23**, 682–732.

20 (*a*) Y. Che, X. Yang, Z. Zhang, J. Zuo, J. S. Moore and L. Zang, *Chem. Commun.*, 2010, **46**, 4127–4129; (*b*) H. Huang, D. E. Gross, X. Yang, J. S. Moore and L. Zang, *ACS Appl. Mater. Interfaces*, 2013, **5**, 7704–7708.

21 (*a*) A. J. Maliakal, J. Y. C. Chen, W.-Y. So, S. Jockusch, B. Kim, M. F. Ottaviani, A. Modelli, N. J. Turro, C. Nuckolls and A. P. Ramirez, *Chem. Mater.*, 2009, **21**, 5519–5526; (*b*) X. Zhang, J. Jie, W. Zhang, C. Zhang, L. Luo, Z. He, X. Zhang, W. Zhang, C. Lee and S. Lee, *Adv. Mater.*, 2008, **20**, 2427–2432.